J. Magn. Soc. Jpn., **47**, 137-143 (2023) <Paper>

Magneto-optical spectroscopy of epitaxial $Co_xFe_{3-x}O_4$ (001) thin films

S. Wang, H. Onoda*, J. Harbovsky**, H. Yanagihara*, J. Inoue*, M. Veis**, and T. Ishibashi
Department of Materials Science and Technology, Nagaoka Univ. of Tech., *1603-1 Kamitomioka, Nagaoka 940-2188, Japan*
* Department of Applied Physics, Univ. of Tsukuba, *1-1-1 Tennodai, Tsukuba 305-0006, Japan*
** Institute of Physics, Charles Univ., *Prague 12116, Czech Republic*

The magneto-optical (MO) spectra of spinel cobalt ferrite thin films with different distortions were measured in a broad range of 0.59 – 3.54 eV. Instead of using the cation substitution method, we prepared cobalt ferrite thin films with local distortion by using a RF magnetron sputtering method on an Mg_2SnO_4 buffer layer to induce epitaxial strain. We derived the diagonal and off-diagonal elements of the dielectric tensor to investigate the influence of distortion on the MO effect in the films. In the spectra of the off-diagonal dielectric elements, the transitions at 0.8, 1.8, and 2.0 eV, which correspond to the optical transitions of tetrahedral (Co^{2+}) and octahedral [Co^{2+}], [Fe^{3+}], were assigned to crystal field (CF) transitions: (Co^{2+}): ${}^4A_2 \rightarrow {}^4T_1$(F), ${}^4A_2 \rightarrow {}^4T_1$(P) and intervalence charge transfer (IVCT) transition: [Co^{2+}]t_{2g} → [Fe^{3+}]t_{2g}, respectively. This result revealed that the Co ions were present in both the tetrahedral and octahedral sites in the epitaxial CFO thin films. By comparing the relative amplitude of each MO transition of cobalt ferrite thin films with different distortions, we found that MO spectroscopy is a highly promising tool for evaluating local distortions.

Keywords: magneto-optical spectroscopy, cobalt ferrite, thin films, dielectric tensor, magnetic anisotropy

1. Introduction

Recently, it has been reported that a giant perpendicular magnetic anisotropy (PMA) was induced by a tetragonal distortion in epitaxially grown spinel $Co_{0.75}Fe_{2.25}O_4$ thin films [1)–5)]. A large PMA energy (K_u = 1.47 MJ/m^3) of $Co_{0.75}Fe_{2.25}O_4$ thin films grown on a MgO (001) substrate was obtained undergoing 0.7% lattice mismatch [2)]. Furthermore, a larger strain was introduced into the $Co_{0.75}Fe_{2.25}O_4$ thin film by introducing Mg_2SnO_4 (MSO) buffer layers with 3.1% lattice mismatch [5),6)], resulting that a giant PMA energy of 6.1 MJ/m^3 was induced by a large epitaxial strain [6)]. This value is much larger than that of the Nd magnet, 4.9 MJ/m^3 [7)]. Understanding the origin of the large magnetic anisotropy (MA) energy is crucial for enhancing the performance of permanent magnets.

The theory predicts that the MA energy of $Co_xFe_{3-x}O_4$ (CFO) is dependent on the distortion of the octahedral structure in which Co^{2+} ions reside [8)]. To investigate the local structure of CFO and its impact on MA, various methods have been utilized, including X-ray magnetic circular dichroism (XMCD), X-ray magnetic linear dichroism (XMLD) spectroscopy, and magneto-optical (MO) spectroscopy. The XMCD and XMLD spectra of epitaxial $Co_xFe_{3-x}O_4$ (x=0.2, 0.6) thin films, prepared by pulsed laser deposition method, revealed that the substantial MA energy originates from the large orbital magnetic moments of distorted octahedron including Co^{2+} ($3d^7$), and no signals of tetrahedral Co^{2+} were detected [9)]. In contrast, MO spectroscopy is a convenient method for studying the electronic structure of materials without the use of a large facility for X-ray source. Numerous studies on MO spectroscopy of spinel CFO have been reported [10)–22)]. Unlike most spinel ferrites such as Fe_3O_4, $MgFe_2O_4$, $Li_{0.5}Fe_{2.5}O_4$ and $NiFe_2O_4$, the MO spectrum of spinel CFO features distinct transitions in visible region and near-infrared region, due to Co ions in tetrahedral and octahedral sites [15)]. As a result, the MO spectroscopy has a potential to be utilized to evaluate the local structure of CFO thin films.

Previous studies on MO spectroscopy of ferrites have revealed that the disturbed local symmetry can alter the MO spectrum by the substitution of nonmagnetic cations for Fe ions in spinel Fe_3O_4 [22),23)] and $CoFe_2O_4$ [24)–26)]. However, substituting other cations affect not only the local symmetry but also the compositions resulting in a change in their magnetic properties, meaning that MO spectra are influenced by more than one factor. In contrast, our study focuses on the effect of distortion on the MO spectroscopy of CFO thin films without changing compositions. To solve these problems, we studied $Co_{0.75}Fe_{2.25}O_4$ thin films with different levels of distortion by introducing an MSO buffer layer on MgO (001) substrate via RF magnetron sputtering. MO spectra of epitaxial spinel-type CFO thin films over a wide energy range (0.59 – 3.54 eV) have been measured for the first time. Dielectric tensor of $Co_{0.75}Fe_{2.25}O_4$ thin films were investigated. Finally, the relationship between local strain and each optical transition was discussed.

2. Dielectric tensor

The Faraday and Kerr spectra of magnetic thin films are dependent on the incident angle and orientation of magnetization, and thus do not represent an intrinsic response. In contrast, the dielectric tensor directly reflects the electronic structure and the transition matrix

Corresponding author: T. Ishibashi (e-mail: t_bashi@mst.nagaokaut.ac.jp).

of optical transitions. For a uniaxial anisotropy with magnetization in the z-direction, the dielectric tensor has the following form,

$$\varepsilon = \begin{pmatrix} \varepsilon_{xx} & -\varepsilon_{xy} & 0 \\ \varepsilon_{xy} & \varepsilon_{xx} & 0 \\ 0 & 0 & \varepsilon_{zz} \end{pmatrix}, \quad (1)$$

where the diagonal element $\varepsilon_{xx} = \varepsilon'_{xx} + i\varepsilon''_{xx}$ and the off-diagonal element $\varepsilon_{xy} = \varepsilon'_{xy} + i\varepsilon''_{xy}$.

The real and imaginary part of ε_{xx} and ε_{xy} can be expressed in terms of refractive index n, the extinction coefficient κ, Faraday rotation θ_F, and Faraday ellipticity η_F as follows [27],

$$\varepsilon'_{xx} = n^2 - \kappa^2, \quad (2)$$

$$\varepsilon''_{xx} = 2n\kappa, \quad (3)$$

$$\varepsilon'_{xy} = \frac{\lambda}{\pi\zeta}(n\eta_F - \kappa\theta_F), \quad (4)$$

$$\varepsilon''_{xy} = \frac{\lambda}{\pi\zeta}(n\theta_F + \kappa\eta_F), \quad (5)$$

where λ is a wavelength and ζ is a thickness of a sample.

From equations (4) and (5), we know that the off-diagonal elements relate to the magnetic properties, and the off-diagonal elements can be determined by measuring the Faraday rotation and ellipticity.

In this study, we used the Lorentz functions to decompose the off-diagonal dielectric tensor elements to each transition, where the diamagnetic and paramagnetic transitions were considered [28]. The expression of diamagnetic transition is described as,

$$\varepsilon(\omega) = A \cdot \frac{2(\omega_0 - \omega) * \Gamma - i((\omega_0 - \omega)^2 - \Gamma^2)}{\omega * ((\omega_0 - \omega)^2 + \Gamma^2)^2}, \quad (6)$$

and the paramagnetic transition is expressed as,

$$\varepsilon(\omega) = A \cdot \frac{2\omega_0\Gamma - i\omega_0(\omega_0{}^2 - \omega^2 + \Gamma^2)}{(\omega_0^2 - \omega^2 + \Gamma^2)^2 + 4\omega^2\Gamma^2}, \quad (7)$$

where A is transition amplitude, ω_0 is resonance frequency, and Γ is a half width at half maximum.

3. Experiments

3.1 Sample preparation and characterizations

We prepared two CFO samples, one of CFO thin films grown on a MgO (001) substrate, and another CFO thin film grown on an MSO buffer layer on the MgO (001) substrate. CFO thin film with a thickness of 20 nm was prepared on MgO (001) substrates as CFO/MgO by the reactive RF magnetron sputtering technique using CoFe (1:3 atomic ratio) alloy targets. To change the distortion of CFO thin films, an MSO buffer layer of 7 nm thickness were grown on single crystal MgO (001) substrates at 600 °C by the reactive RF magnetron sputtering using Mg and Sn metal targets under 0.5 Pa pressure of Ar and O_2 mix gas. Then the MSO film was post-annealed at 1000 °C for 10 min in air. CFO thin film with a thickness of 20 nm was grown on the post-annealed MSO films and MgO substrate as CFO/MSO/MgO at 500 °C using a CoFe (1:3 atomic ratio) metal alloy, under 0.5 Pa pressure of Ar and O_2 mix gas.

Magnetization curves were measured by a superconducting quantum interference device, SQUID-VSM (Quantum Design, MPMS), at fields up to ± 9 T. Thicknesses of CFO thin films were determined a spectroscopic ellipsometer (M-2000DI-YK, J.A.Woollam). The crystallinity of prepared CFO thin films was characterized by the X-ray diffractometer (Rigaku, SmartLab) using CuKα_1 radiation (λ = 0.154059 nm) for out-of-plane measurements and CoKα_1 radiation (λ = 0.178900 nm) for in-plane measurement monochromized with a double Ge (220) monochromator.

3.2 Measurements of optical and MO properties of CFO thin films

To investigate the complete dielectric tensor, we used an ellipsometer to determine the diagonal element, and the off-diagonal tensor were derived by spectroscopic ellipsometry and MO spectroscopy. The optical properties were measured by spectroscopic ellipsometry for an energy range between 0.73 – 6.02 eV (206 – 1690 nm), RC2 (J.A.Woollam). The diagonal dielectric elements were fitted with the Tauc-Lorentz model using the CompleteEASE (J. A. Wollam Co., Inc.) software. MO spectra ranging from 0.59 – 3.54 eV (350 – 2100 nm) were measured by a multi-channel MO spectrometer [29].

The MO spectrometer used in this study was shown in Fig. 1. All optical components of the MO spectrometer were set on an ordinary optical table. The optical setup includes a light source, a polarizer, a quarter-wave plate, an electromagnet (Max filed: ± 1.7 T), an analyzer, a detector, and three collimate lenses. A halogen lamp (U-LH100L-3, TH4-100, Olympus Inc.) with a power of 100 W was used as a light source. A spatial filter was set in front of the light source, with a variable pinhole in the focal point of the two N-BK7 plano-convex lenses L1 and L2 (Transmittance > 80% at 350 – 2100 nm). Two Glan-Thompson prisms with an extinction ratio of 1×10^5 were used as a polarizer and an analyzer. Two types of achromatic quarter-wave plates, SAQWP05M-700 (Thorlabs Inc.) for 325 – 1100 nm and SAQWP05M-1700 (Thorlabs Inc.) for 600 – 2700 nm, were used in the measurement of ellipticity. Two types of multi-channel spectrometers were used. The USB2000+VIS-NIR (Ocean Optics Inc., wavelength range: 350 – 1000 nm) spectrometer with a 2048-element linear silicon CCD array detector (ILX511B, Sony Inc.) was used for the visible light, and the NIRQUEST512-2.5 (Ocean Optics

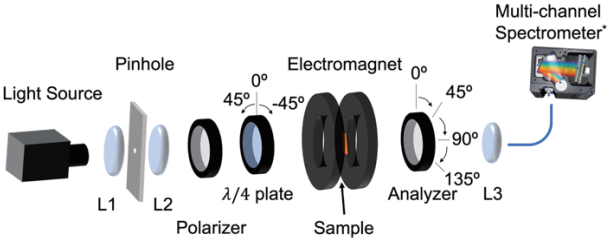

Fig. 1 Illustration of MO multi-channel spectrometer using Stokes parameter method. *USB2000 + VIS-NIR, NIRQUEST512-2.5 (Ocean Optics Inc.)

Inc., wavelength range: 900 – 2500 nm) with a 512-element InGaAs linear array image sensor (G9208-512W, Hamamatsu Photonics K.K.) was used for the near-infrared light. The transmitted light from the analyzer was focused by the collimation lens L3 into an optical fiber connected to the multi-channel spectrometer. The effective measurement range of the MO spectra is considered between 350 and 2100 nm (3.54 – 0.59 eV) according to the above configurations.

In the process of MO measurement, the polarization axis of the polarizer was fixed to the vertical plane as 0° all the time, and the analyzer and the quarter wave-plate are rotated by a stepping motor (DS102, Suruga Seiki). The magnetic field was applied perpendicular to the sample up to 1.7 T by a double-yoked electromagnet.

To measure the Faraday rotation and Faraday ellipticity spectra, we measured Stokes parameters, defined by azimuth angle θ and ellipticity η as described by

$$\begin{pmatrix} s_0 \\ s_1 \\ s_2 \\ s_3 \end{pmatrix} = \begin{pmatrix} 1 \\ \cos 2\eta \cos 2\theta \\ \cos 2\eta \sin 2\theta \\ \sin 2\eta \end{pmatrix}. \quad (8)$$

In this case, azimuth θ can be expressed as an equation,

$$\theta = \frac{1}{2}\tan^{-1}\left(\frac{s_2}{s_1}\right) = \frac{1}{2}\tan^{-1}\left(\frac{I_{45^\circ} - I_{135^\circ}}{I_{0^\circ} - I_{90^\circ}}\right), \quad (9)$$

where I_{0°, I_{45°, I_{90°, and I_{135° are optical intensities measured with the analyzer angles of 0°, 45°, 90°, and 135°, respectively. For measuring the Faraday ellipticity spectra, the analyzer is fixed to 0°, and the fast axis of the quarter wave-plate is rotated to –45°, +45° with the polarizer, corresponding to left-handed circular polarization (LCP), and right-handed circular polarization (RCP), respectively. Ellipticity η can be expressed by,

$$\eta = \frac{1}{2}\sin^{-1}\left(\frac{s_3}{s_0}\right) = \frac{1}{2}\sin^{-1}\left(\frac{I_{LCP} - I_{RCP}}{I_{LCP} + I_{RCP}}\right), \quad (10)$$

where I_{LCP} and I_{RCP} are the intensities at the detector obtained with polarization states of LCP, and RCP.

Using the above method and a multi-channel spectrometer, Faraday rotation and Faraday ellipticity spectra can be acquired within a mere 5 minutes. To ensure accuracy, all Faraday spectra are averaged in opposite magnetic field directions and calibrated [29),30)], effectively removing any offset due to the optical setup. The measurement of Faraday rotation and ellipticity spectra was conducted at room temperature.

4. Results and discussion

X-ray diffraction (XRD) patterns of CFO/MgO and CFO/MSO/MgO measured in both in-plane and out-of-plane orientations are shown in Fig. 2. In Fig. 2 (a), diffraction peaks observed at $2\theta = 95.20°$ for CFO/MgO and 95.59° for CFO/MSO/MgO correspond to the 008 diffractions of CFO with the spinel-type structure with c = 0.8345 and 0.8319 nm, respectively. In-plane lattice constants of CFO thin films are determined from CFO (220) diffractions in Fig. 2 (b) to be a = 0.8425 nm for CFO/MgO and a = 0.8439 nm for CFO/MSO/MgO. Compared to the lattice constant of bulk CFO (a = 0.838 nm), out-of-plane compressive strains of CFO thin films in CFO/MgO and CFO/MSO/MgO were determined to be $\varepsilon_\perp = -0.418\%$ and $\varepsilon_\perp = -0.728\%$, while in-plane tensile strains were $\varepsilon_\parallel = 0.537\%$ and $\varepsilon_\parallel = 0.704\%$ for CFO/MgO and CFO/MSO/MgO, respectively. These values are comparable to those reported previously [2),5)]. The total distortions χ of CFO thin films were defined as $\chi = \varepsilon_\parallel - \varepsilon_\perp$ [6)], 0.955% and 1.432% for CFO/MgO and CFO/MSO/MgO. These results indicated that both CFO thin films are distorted by the lattice mismatch. The larger distortion in CFO/MSO/MgO was induced by the MSO buffer layer with larger lattice constant compared to the MgO substrate. Additionally, Laue oscillation was observed in the XRD pattern for the CFO/MgO sample shown in Fig. 2 (a), indicating excellent crystallinity and a smooth surface of CFO thin films. Postannealed MSO layer was investigated by reflection high-energy electron diffraction (RHEED) and cross-sectional transmission electron microscopy (TEM) previously, indicating that MSO layer is single crystal with a flat surface [6)].

Fig. 3 shows magnetization curves of CFO thin films, which were measured with magnetic fields applied perpendicular to the plane. The saturation magnetization (M_s) was measured to be 395 kA/m for both CFO/MgO and CFO/MSO/MgO thin films, which

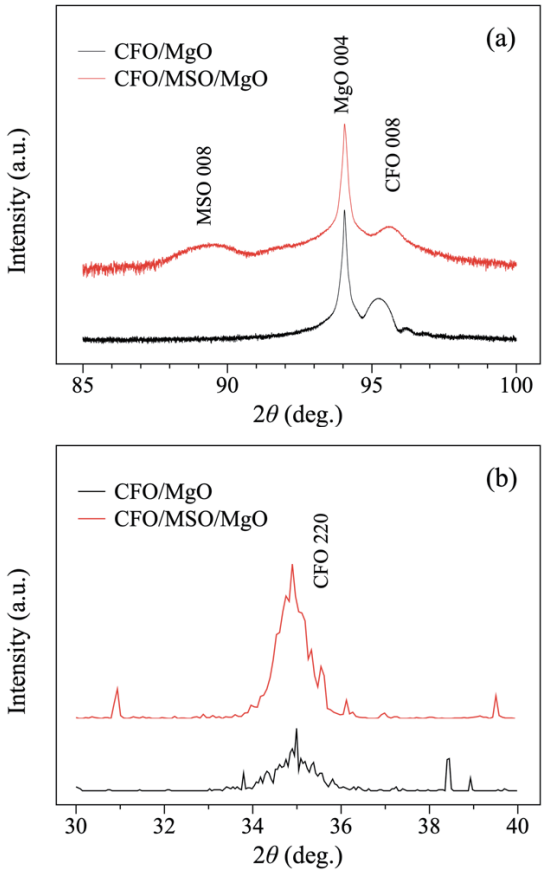

Fig. 2 XRD patterns of CFO/MgO and CFO/MSO/MgO. (a) Out-of-plane patterns in range of 85 – 100°, (b) In-plane patterns in range of 30 – 40°.

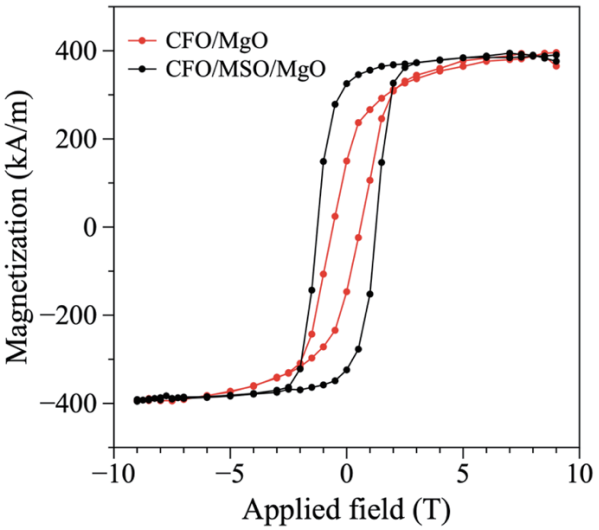

Fig. 3 Out-of-plane hysteresis loop of CFO thin films prepared on MgO and MSO/MgO substrates, measured by SQUID magnetometry.

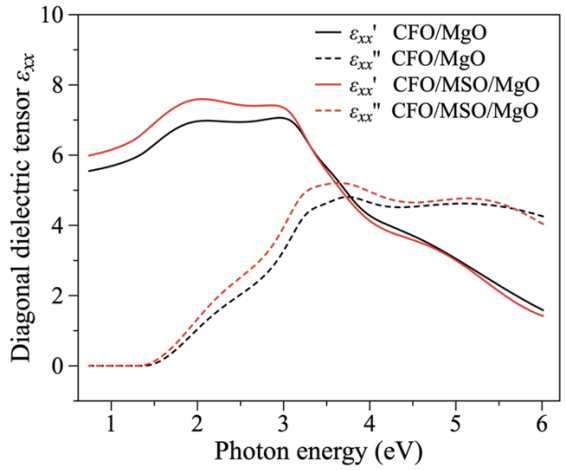

Fig. 4 Diagonal elements of dielectric tensor of CFO thin films on MgO and MSO/MgO.

was close to that of bulk CFO crystal, 425 kA/m [2]. The fact that the CFO thin films have M_s comparable to that of bulk CFO crystal suggests that the distortion has not significantly affected the saturation magnetization. On the other hand, the CFO/MgO and CFO/MSO/MgO thin films exhibited different coercive fields of 5.94 A/m and 12.63 A/m, respectively, depending on the distortion. These characteristics of these CFO thin films used in this study is consistent with previous reports [5),6)].

The diagonal elements of dielectric tensor ε'_{xx} and ε''_{xx} of CFO thin films are shown in Fig. 4. Five oscillators were considered to fit the imaginary part of diagonal elements of the dielectric tensor of these CFO thin films, where the parameters used for the fitting are listed in Table 1. Thicknesses of the CFO thin films were determined to be 25.27 ± 0.03 nm for CFO/MgO and 22.47 ± 0.09 nm for CFO/MSO/MgO, respectively. Thicknesses of the MSO buffer layer was determined to be 7.00 ± 0.39 nm. Postannealed MSO layer was also investigated, resulting in a roughness of 1.05 nm, which indicates that

Table 1 Parameters used to fit diagonal elements ε''_{xx} of CFO thin films on MgO and MSO/MgO. Lists are peak position ω_0 (eV), full width at half maximum Γ (eV), amplitude A of each oscillator (Osc.).

Sample		Osc. 1	Osc. 2	Osc. 3	Osc. 4	Osc. 5
CFO/MgO	ω_0	2.17	3.24	3.71	5.53	9.04
	Γ	1.97	0.59	1.53	3.23	0.0001
	A	15.509	1.495	9.403	21.694	11.468
CFO/MSO/MgO	ω_0	2.25	3.21	3.69	5.51	7.78
	Γ	1.96	0.64	1.50	3.28	0.41
	A	16.327	1.933	9.038	21.613	3.859

the MSO has a flat surface. The fitting was carried out with small mean squared error (MSE) of 1.669 for CFO/MgO and 2.025 for CFO/MSO/MgO. The real part of diagonal elements ε'_{xx} of CFO thin films showed a broad structure with two dominant peaks at 1.9 and 3.0 eV. The imaginary part of diagonal elements ε''_{xx} showed that a broad absorption from 1.3 eV. It was found that the ε'_{xx} of CFO/MgO is lower than that of CFO/MSO/MgO between 0.73 and 3.1 eV. For ε''_{xx}, the intensity of CFO/MSO/MgO is larger than that of CFO/MgO between 1.5 – 4.5 eV. These differences can be attributed to the enhancement of optical absorption caused by the increased distortion of CFO thin films.

Fig. 5 shows the Faraday rotation and ellipticity spectra of the CFO thin films in range of 0.59 to 3.54 eV. Faraday spectra of MgO (001) substrate and MSO buffer layer measured under the same magnetic field were subtracted from the measured spectra to eliminate the influence of the Faraday effect. As the applied magnetic field cannot fully saturate both samples in these measurements, the MO spectra with fully saturated were estimated. Using the magnetic hysteresis loop, the estimated MO spectra were obtained by multiplying coefficients of 1.53 and 2.16 for CFO/MgO and CFO/MSO/MgO, respectively, where those coefficients were obtained by a ratio of a magnetization measured at 1.7 T and a saturation magnetization.

The Faraday spectra are in good agreement with those of the bulk spinel $CoFe_2O_4$ [10),14)]. Both CFO thin films exhibited a broad intense negative peak between 1.3 and 2.8 eV and a narrow dispersion-type transition at 0.8 eV. Although the transition energies did not change, the intensity of the rotation and ellipticity spectra increases significantly in the CFO/MSO/MgO. To understand the microscopic origin of the MO effect, we have derived the off-diagonal elements ε_{xy} of the dielectric tensor using equations (4) and (5).

Fig. 6 shows the spectra of real part and imaginary part of ε_{xy} of the CFO thin films in the region between 0.73 and 3.54 eV. The structures of ε_{xy} of CFO thin films are in good agreement with the previous MO study on bulk CFO crystals [10)]. To evaluate each optical transition, we fitted the real part of the off-diagonal dielectric tensor element ε'_{xy} using equations (6) and (7).

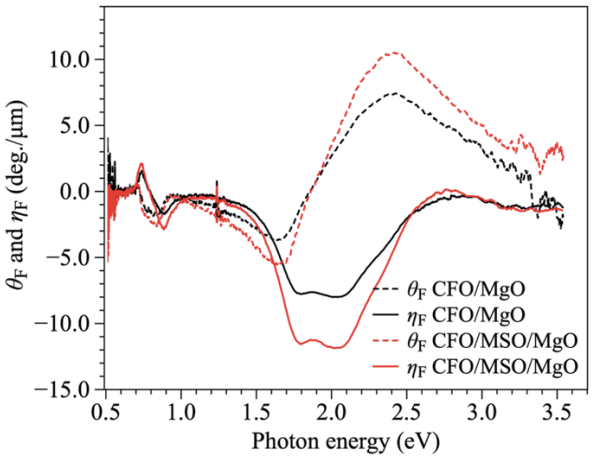

Fig. 5 Faraday rotation θ_F and ellipticity η_F spectra of CFO/MgO and CFO/MSO/MgO.

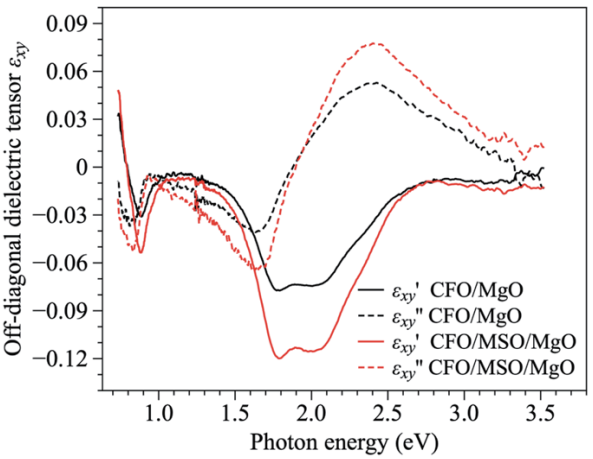

Fig. 6 Off-diagonal elements of dielectric tensor of CFO thin films on CFO/MgO and CFO/MSO/MgO.

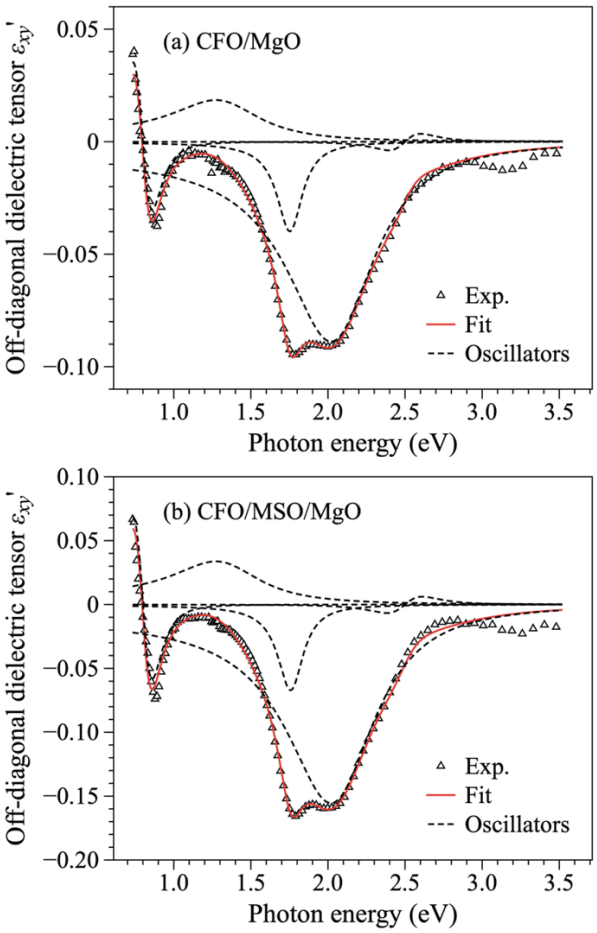

Fig. 7 Fitting to real part of off-diagonal dielectric tensor elements of CFO thin films. (a) CFO/MgO, (b) CFO/MSO/MgO.

The assignment of MO transitions was based on previous MO spectroscopic studies of CFO [10),15),22)]. The fitting results are presented in Fig. 7. The fitting parameters, including the transition amplitude A, peak position ω_0 (eV), and half width at half maximum Γ (eV), are summarized in Table 2. Five MO transitions at 0.80, 1.32, 1.76, 2.05, and 2.50 eV were considered for both two CFO thin films.

The MO spectra exhibited a diamagnetic transition characterized by two peaks of opposite sign at 0.80 eV in the low photon energy region, as well as a paramagnetic transition featuring a single negative peak at 1.76 eV. These transitions are similar to those reported in Ref. [31)], where optical transitions were found at 0.86 and 1.98 eV corresponded to two types of crystal-field (CF) transitions of tetrahedral Co^{2+}: $^4A_2 \rightarrow {}^4T_1$(F) and $^4A_2 \rightarrow {}^4T_1$(P) in Co-doped ZnO single crystals. Therefore, we assigned the diamagnetic transitions at 0.80 eV to the CF transition of Co^{2+}: $^4A_2 \rightarrow {}^4T_1$(F), and the paramagnetic transition at 1.76 eV was assigned to the CF transition of Co^{2+}: $^4A_2 \rightarrow {}^4T_1$(P). An intense broad paramagnetic transition at 2.05 eV is assigned to an IVCT transition: $[Co^{2+}]t_{2g} \rightarrow [Fe^{3+}]t_{2g}$, as identified by Peeters and Martens in polycrystalline bulk CFO [13)]. A weak diamagnetic transition is observed at 2.50 eV with two opposite peaks, consistent with a previously reported transition at 2.6 eV in bulk spinel Fe_3O_4 [23)], and assigned to an ISCT transition: $(Fe^{3+})t_2 \rightarrow [Fe^{2+}]t_{2g}$. Additionally, our fitting results obtained a broad paramagnetic transition at 1.32 eV with a positive peak, which has not be previously discussed in CFO. However, the exact assignment of this transition cannot be confirmed in this study. It might be related to a CF transition of tetrahedral Co^{3+}: $^5E \rightarrow {}^5T_2$, as reported in $(YGd)_3(Co_xFe_{5-x})O_{12}$ thin films at 0.95 eV [32),33)], but further investigation is needed to confirm this transition in CFO.

The IVCT transition of $[Co^{2+}]t_{2g} \rightarrow [Fe^{3+}]t_{2g}$ and the CF transitions of (Co^{2+}): $^4A_2 \rightarrow {}^4T_1$(F) and $^4A_2 \rightarrow {}^4T_1$(P) associated with octahedral and tetrahedral sites were observed in both samples, as previously assigned. This result suggests that Co^{2+} is not only present in the octahedral site but also in the tetrahedral site. Previous studies have indicated that the Co cations only exist in the octahedral sites for epitaxial CFO thin films [6),9)]. However, our finding demonstrates that the epitaxial $Co_{0.75}Fe_{2.25}O_4$ thin film is not a complete inverse-spinel structure, despite having a lower Co composition than $CoFe_2O_4$. Previous interpretations of the MA in epitaxial CFO as originating solely from the large orbital magnetic

Table 2 Optical transitions of CFO thin films on CFO/MgO and CFO/MSO/MgO between 0.73 and 3.54 eV. Lists are peak position ω_0 (eV), half width at half maximum Γ (eV), amplitude A, and assignment of each transition. Tetrahedral and octahedral sites are denoted by ( ) and [ ], respectively.

Type		CF	CF	CF	IVCT	ISCT
Assignment		(Co^{2+}): $^4A_2 \rightarrow {}^4T_1$(F)	(Co^{3+}): $^5E \rightarrow {}^5T_2$	(Co^{2+}): $^4A_2 \rightarrow {}^4T_1$(P)	$[Co^{2+}]t_{2g}$ $\rightarrow [Fe^{3+}]t_{2g}$	(Fe^{3+}) t_2 $\rightarrow [Fe^{2+}]t_{2g}$
Shape		dia	para	para	para	dia
CFO/MgO	ω_0	0.80	1.32	1.76	2.05	2.50
	Γ	0.11	0.35	0.10	0.35	0.18
	A	0.0010	0.0342	-0.0280	-0.2550	-0.0009
CFO/MSO/MgO	ω_0	0.80	1.32	1.76	2.05	2.50
	Γ	0.11	0.35	0.10	0.35	0.20
	A	0.0019	0.0624	-0.0473	-0.4463	-0.0020

moment of the octahedral Co^{2+} due to epitaxial strain [9),34)], ignoring the effect of tetrahedral Co^{2+}. However, we have found that Co^{2+} is also present in tetrahedral site in epitaxial CFO thin films, suggesting that the origin of PMA in epitaxial CFO thin films needs to be re-evaluated.

Compared to the MO spectra of these two CFO thin films, we noticed a significant increase in the transition amplitude of all MO transitions in CFO/MSO/MgO. The IVCT transition $[Co^{2+}]t_{2g} \rightarrow [Fe^{3+}]t_{2g}$ amplitude increased 1.75 times from –0.2550 in CFO/MgO to –0.4463 in CFO/MSO/MgO. Similarly, the transition amplitude of the CF transition (Co^{2+}): $^4A_2 \rightarrow {}^4T_1$(F) at 0.86 eV increased 1.90 times from –0.0010 in CFO/MgO to –0.0019 in CFO/MSO/MgO. We attribute the alteration of the IVCT transition to the octahedral symmetry perturbation caused by the epitaxial tensile strain. This perturbation increases the distance between $[Fe^{3+}]$ and $[Co^{2+}]$ for adjacent octahedral sites along the a-axis. As the oscillator strength of the IVCT transition is sensitive to changes in the lattice, the longer lattice constant of the CFO leads to a decrease in the transition amplitude of the IVCT transition $[Co^{2+}]t_{2g} \rightarrow [Fe^{3+}]t_{2g}$, as reported by Fontijn et al.[23)].

Additionally, an increase in the CF transition (Co^{2+}): $^4A_2 \rightarrow {}^4T_1$(F) at 0.86 eV in CFO/MSO/MgO was observed, with an amplitude 1.75 times higher than that of tetrahedral Co^{2+} in CFO/MgO. We considered that this increase is attributed to the perturbation of the tetrahedral symmetry caused by the epitaxial tensile strain, which affects not only the octahedral symmetry but also the trigonal symmetry of the tetrahedral structure [23)]. Calculation results have shown that the Co L_{23}-edge absorption in the tetrahedral symmetry increases with the increasing crystal field [35)], which is consistent with our results. Our findings suggest that the distorted tetrahedral symmetry in CFO thin films enhances the tetrahedral CF transitions.

Finally, we compared the intensity ratios of the octahedral transition ($[Co^{2+}]t_{2g} \rightarrow [Fe^{3+}]t_{2g}$) to the tetrahedral transition ((Co^{2+}): $^4A_2 \rightarrow {}^4T_1$(F)) in CFO/MgO and CFO/MSO/MgO. The ratio was found to be 1 : 0.34 for CFO/MgO and 1 : 0.37 for CFO/MSO/MgO. The slight difference in ratio may be explained by the different cation distributions caused by the distortion. Frisch et al.[36)] reported that the epitaxial tensile strain reduces inversion, which shift Co from the octahedral site to the tetrahedral site. This shift results in an increase in the tetrahedral transition compared to the octahedral transition. Therefore, the enhanced tetrahedral transition intensity in CFO/MSO/MgO is consistent with the cation distribution changes induced by epitaxial tensile strain as reported by Frisch et al.[36)]. However, further research is necessary to quantitative evaluate the composition of CFO.

5. Conclusion

We investigated two types of high-quality spinel-type CFO thin films prepared on MgO and MSO/MgO substrates by the RF magnetron sputtering method, which had different strains of 0.955% and 1.432%, respectively, induced by lattice mismatching. Dielectric tensors of those CFO thin films were deduced from the optical and Faraday spectra. By observing MO transitions of tetrahedral (Co^{2+}) and octahedral $[Co^{2+}]$ in both samples, we revealed that Co ions are present in both tetrahedral and octahedral sites in the epitaxial CFO thin films. Furthermore, comparison of the amplitude of each transition indicated that the induced tensile strain leads to an enhancement of MO transitions in CFO thin films. Our results suggest that the MO spectroscopy serves as a sensitive tool for qualitatively investigating cation distribution in CFO thin films, demonstrating the potential for qualitative evaluation of local strain and laying the groundwork for future quantitative analyses of local strain in CFO thin films.

Acknowledgements The authors acknowledge funding from the Japan Science and Technology Agency (JST)

under Collaborative Research Based on Industrial Demand "High-Performance Magnets: Toward Innovative Development of Next-Generation Magnets" under Grant JPMJSK1415. We also thank Prof. Asada and Dr. Kimura for the measurement of the ellipsometry at the Center for Instrumental Analysis, Yamaguchi University.

References

1) A. Lisfi, C. M. Williams, L. T. Nguyen, J. C. Lodder, A. Coleman, H. Corcoran, A. Johnson, P. Chang, A. Kumar, and W. Morgan: *Phys. Rev. B*, **76**, 054405 (2007).
2) T. Niizeki, Y. Utsumi, R. Aoyama, H. Yanagihara, J. Inoue, Y. Yamasaki, H. Nakao, K. Koike, and E. Kita: *Appl. Phys. Lett.*, **103**, 162407 (2013).
3) H. Yanagihara, Y. Utsumi, T. Niizeki, J. Inoue, and E. Kita: *J. Appl. Phys.*, **115**, 17A719 (2014).
4) H. Onoda, H. Sukegawa, E. Kita, and H. Yanagihara: *IEEE Trans. Magn.*, **54**, 2502104 (2018).
5) H. Onoda, H. Sukegawa, and H. Yanagihara: *IEEE Trans. Magn.*, **56**, 1 (2020).
6) H. Onoda, H. Sukegawa, J. Inoue, and H. Yanagihara: *Adv. Mater. Interfaces*, **8**, 2101034 (2021).
7) M. Sagawa, S. Hirosawa, H. Yamamoto, S. Fujimura, and Y. Matsuura: *Jpn. J. Appl. Phys.*, **26**, 785 (1987).
8) J. Inoue, H. Yanagihara, and E. Kita: *Mater. Res. Express*, **1**, 046106 (2014).
9) J. Okabayashi, M. A. Tanaka, M. Morishita, H. Yanagihara, and K. Mibu: *Phys. Rev. B*, **105**, 134416 (2022).
10) J. W. D. Martens, W. L. Peeters, H. M. van Noort, and M. Erman: *J. Phys.& Chem. Solids*, **46**, 411 (1985).
11) N. Evtihiev, N. Economov, A. Krebs, N. Zamjatina, V. Baurin, and V. Pinko: *IEEE Trans. Magn.*, **12**, 773 (1976).
12) J. W. D. Martens and A. Voermans: *IEEE Trans. Magn.*, **20**, 1007 (1984).
13) W. L. Peeters and J. W. D. Martens: *J. Appl. Phys.*, **53**, 8178 (1982).
14) L. Stichauer, G. Gavoille, and Z. Simsa: *J. Appl. Phys.*, **79**, 3645 (1996).
15) W. F. J. Fontijn, P. J. van der Zaag, and R. Metselaar: *J. Appl. Phys.*, **83**, 6765 (1998).
16) K. J. Kim, M. H. Lee, and S. H. Lee: *J. Appl. Phys.*, **91**, 9974 (2002).
17) Y. A. Gromova, V. G. Maslov, M. A. Baranov, R. Serrano-García, V. A. Kuznetsova, F. Purcell-Milton, Y. K. Gun'ko, A. V. Baranov, and A. V. Fedorov: *J. Phys. Chem. C*, **122**, 11491 (2018).
18) B. S. Holinsworth, N. C. Harms, S. Fan, D. Mazumdar, A. Gupta, S. A. McGill, and J. L. Musfeldt: *APL Mater.*, **6**, 066110 (2018).
19) R. Illa, R. Ješko, R. Silber, O. Životský, K. M. Kutláková, L. Matějová, M. Kolenčík, J. Pištora, and J. Hamrle: *Mater. Res. Bull.*, **117**, 96 (2019).
20) J. W. D. Martens: *J. Appl. Phys.*, **59**, 3820 (1986).
21) K. Yasuda, M. Nishikawa, and T. Ishibashi: *Jpn. J. Appl. Phys.*, **59**, SEEA01 (2020).
22) W. F. J. Fontijn, P. J. van der Zaag, L. F. Feiner, R. Metselaar, and M. A. C. Devillers: *J. Appl. Phys.*, **85**, 5100 (1999).
23) W. F. J. Fontijn, P. J. van der Zaag, M. A. C. Devillers, V. A. M. Brabers, and R. Metselaar: *Phys. Rev. B*, **56**, 5432 (1997).
24) B. Zhou, Y. Zhang, Y. Yu, C. Liao, C. Yan, L. Chen, and S. Wang: *Phys. Rev. B*, **68**, 024426 (2003).
25) B. Zhou, Y. Zhang, C. Liao, F. Cheng, C. Yan, L. Chen, and S. Wang: *Appl. Phys. Lett.*, **79**, 1849 (2001).
26) B. Zhou, Y. Zhang, C. Liao, C. Yan, L. Chen, and S. Wang: *Solid State Commun.*, **126**, 593 (2003).
27) S. Wittekoek, T. J. A. Popma, J. M. Robertson, and P. F. Bongers: *Phys. Rev. B*, **12**, 2777 (1975).
28) J. C. Suits: *IEEE Trans. Magn.*, **8**, 95 (1972).
29) S. Wang, M. Nishikawa, T. Ishibashi, and K. Sato: *Jpn. J. Appl. Phys.*, **59**, SEEA02 (2020).
30) K. Sato, H. Hongu, H. Ikekame, Y. Tosaka, M. Watanabe, K. Takanashi, and H. Fujimori: *Jpn. J. Appl. Phys.*, **32**, 989 (1993).
31) R. Pappalardo, D. L. Wood, and R. C. Linares: *J. Chem. Phys.*, **35**, 2041 (1961).
32) T. Saito, K. Tamanoi, K. Shinagawa, and T. Tsushima: *J. Magn. Soc. Jpn.*, **11** (Suppl. No. S1), 245 (1987).
33) L. McAven and K. Shinagawa: *J. Phys. Condens. Matter*, **14**, 11859 (2002).
34) J. Inoue, H. Onoda, and H. Yanagihara: *J. Phys. D: Appl. Phys.*, **53**, 195003 (2020).
35) M. Wu, X. Huang, K. H. L. Zhang, S. Hu, L. Chen, H.-Q. Wang, and J. Kang: *Phys. Rev. B*, **104**, 075109 (2021).
36) D. Fritsch and C. Ederer: *Appl. Phys. Lett.*, **99**, 081916 (2011).

Received May 14, 2023; Accepted Jul. 18, 2023